JOURNAL OF SYNCHROTRON RADIATION

ISSN 1600-5775

Received 14 July 2016
Accepted 1 March 2017

Edited by I. Schlichting, Max Planck Institute for Medical Research, Germany

Keywords: high pressure; single crystal; XRD.

Supporting information: this article has supporting information at journals.iucr.org/s

A high-pressure single-crystal-diffraction experimental system at 4W2 beamline of BSRF

Xiaodong Li,[a]* Hui Li,[b]* Pengshan Li,[a] Rui Li,[a] Jing Liu,[a] Yanchun Li[a] and Weiran Cui[a]

[a]Beijing Synchrotron Radition Facility, Institute of High Energy Physics, Chinese Academy of Sciences, 19B Yuquan Road, Shijingshan District, Beijing 100049, People's Republic of China, and [b]Institute of Microstructure and Properties of Advanced Materials, Beijing University of Technology, 100 Ping Le Yuan, Chaoyang District, Beijing 100124, People's Republic of China. *Correspondence e-mail: lixd@ihep.ac.cn, huilicn@yahoo.com

Information on the structural evolution of materials under high pressure is of great importance for understanding the properties of materials exhibited under high pressure. High-pressure powder diffraction is widely used to investigate the structure evolution of materials at such pressure. Unfortunately, powder diffraction data are usually insufficient for retrieving the atomic structures, with high-pressure single-crystal diffraction being more desirable for such a purpose. Here, a high-pressure single-crystal diffraction experimental system developed recently at beamline 4W2 of Beijing Synchrotron Radiation Facility (BSRF) is reported. The design and operation of this system are described with emphasis on special measures taken to allow for the special circumstance of high-pressure single-crystal diffraction. As an illustration, a series of diffraction datasets were collected on a single crystal of LaB_6 using this system under various pressures (from ambient pressure to 39.1 GPa). The quality of the datasets was found to be sufficient for structure solution and subsequent refinement.

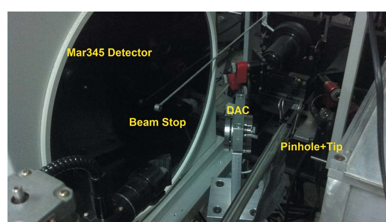

© 2017 International Union of Crystallography

1. Introduction

Pressure has an important effect on the structure and properties of materials. Studies on materials under high pressure may lead to fundamental discoveries of new phases and novel physics and chemistry. Therefore, the development of facilities to perform high-pressure studies has attracted great interest from researchers from diverse fields since the 1970s. Up to now, high-pressure powder diffraction has been the most widely used technique for studying the structure evolution of materials under high pressure (Hemley *et al.*, 1987; Mao *et al.*, 1989, 2006; Chen *et al.*, 2004; Katrusiak, 2008; Akahama & Kawamura, 2010; Ridley & Kamenev, 2014; Shahar *et al.*, 2016). In a typical high-pressure powder diffraction experiment, sample in powder form is loaded in a diamond anvil cell (DAC) to be applied a desired pressure, and then exposed to synchrotron radiation for collection of powder diffraction data. Nevertheless, powder diffraction data have inherent limitations, such as preferred orientation, broadening and overlapping of diffraction peaks, and low signal-to-noise ratios. Single-crystal diffraction data are much more favourable for retrieving structure information because they contain three-dimensional positional information of reflections, and do not suffer from the problems of preferred orientation and overlapping of reflections. Moreover, it is much easier to achieve a good signal-to-noise ratio for single-crystal diffraction than for powder diffraction. Therefore, single-crystal diffraction is particularly preferred over powder diffraction

for sources with low energy and brilliance, such as Beijing Synchrotron Radiation Facility (BSRF) for example. Not only the atomic coordinates of crystals but also small structural distortions, disorders and reliable displacement parameters can usually be well determined from single-crystal diffraction data. Unfortunately, in comparison with regular single-crystal diffraction instruments, high-pressure single-crystal diffraction facilities are much more complex in instrumental design, data collection and reduction due to the presence of the DAC. The main difficulties of high-pressure single-crystal diffraction are as follows. Firstly, the investigated crystals have to be loaded into a chamber formed by diamond anvils and gasket, and immersed in a pressure medium. The completeness and redundancy of the data collected in high-pressure single-crystal diffraction measurements are severely limited due to the shadowing effect of the DAC. To compensate for the insufficient completeness and redundancy, the intensities of the accessible reflections should be determined as accurately as possible. This puts forward higher requests for intensity integration and correction. Secondly, a DAC with a wide opening cone has to be used to alleviate the shadowing effect. Thirdly, the single crystals will usually degrade in quality due to the effect of non-hydrostatic pressure, resulting in much distorted reflections. Lastly, single crystals may be crushed into pieces under high pressure, leading to the superposition of reflections from crystallites with random orientation. Specific algorithms have to be developed to analyse such data.

Up to now, experimental apparatus for high-pressure powder diffraction has been generally available at most synchrotron radiation facilities. Facilities for high-pressure single-crystal diffraction measurements have been developed at a few synchrotron radiation sources, such as the Advanced Photon Source (Shen & Sinogeikin, 2015), SPring-8 (Watanuki *et al.*, 2007), European Synchrotron Radiation Facility (Mezouar *et al.*, 2005) and Petra III (Rothkirch *et al.*, 2013); in comparison with high-pressure powder diffraction facilities, high-pressure single-crystal diffraction systems are much less available at synchrotron radiation sources. Even worse, the facilities for high-pressure single-crystal diffraction are usually inferior to those for high-pressure powder diffraction in terms of usability. In addition to the high-pressure single-crystal diffraction apparatus installed at synchrotron radiation facilities, laboratory apparatus has also been reported. For example, Angel's group have developed apparatus for high-pressure single-crystal diffraction based on a commercially available diffractometer, and achieved some interesting results using such laboratory instruments (Angel, 2004; Ross *et al.*, 2004; Zhao *et al.*, 2010; Angel & Gonzalez-Platas, 2013). Limited by the intensity of the light source, the highest pressure attainable with laboratory apparatus is usually less than 20 GPa (Lager *et al.*, 2002; Ross *et al.*, 2004; Sowa & Ahsbahs, 2006; Zhao *et al.*, 2010; Wu *et al.*, 2013).

Table 1
Specifications of 4W2.

Beamline name	4W2/high pressure
Source type	In-vacuum wiggler
Monochromator	Si(111)
Energy range (keV)	10–25
Energy resolution ($\Delta E/E$)	7×10^{-4}
Beam size at sample (µm)	Single-crystal XRD: 50 (H) × 50 (V) Powder XRD: ∼29 (H) × 8 (V) by KB mirror
Flux at sample position (photons s^{-1})	4×10^7 at 0.6199 Å Focused: 5×10^8 at 0.6199 Å
Detector model	Image plate Mar345, Pilatus3 2M

Due to the difficulties in the development of instruments, few studies on high-pressure single-crystal diffraction have been reported (Hazen *et al.*, 1987; Angel & Finger, 2011; Dera *et al.*, 2011; Posner *et al.*, 2014; Li *et al.*, 2015).

BSRF is a first-generation synchrotron radiation source, which was developed from the late 1980s to early 1990s as a part of the Beijing Electron Positron Collider (BEPC), and upgraded in 2004–2009. BSRF has three experimental halls, five insertion devices and 14 beamlines/endstations. The storage ring operates at 2.5 GeV and 250–150 mA in dedicated synchrotron radiation mode. The beam intensity is constantly 250 mA in top-up mode.

In 2006, experimental apparatus for high-pressure angle-dispersive X-ray powder diffraction was developed at the high-pressure station at the 4W2 beamline of BSRF (Lin *et al.*, 2012; Xiao *et al.*, 2012; Li *et al.*, 2014). To retrieve more information on the structure evolution of materials under high pressure, apparatus was recently installed at the same endstation to collect diffraction data from single crystals in DACs. Here we report the key technical details and the operation of the recently installed experimental system, together with the software specially developed for it. Then diffraction datasets from LaB_6 recorded under various pressures are shown as an example to illustrate the data quality attainable with this facility.

2. Beamline overview

The high-pressure endstation is located at beamline 4W2 of BSRF. A schematic overview of the beamline is shown in Fig. 1, while its parameters are listed in Table 1. The beamline

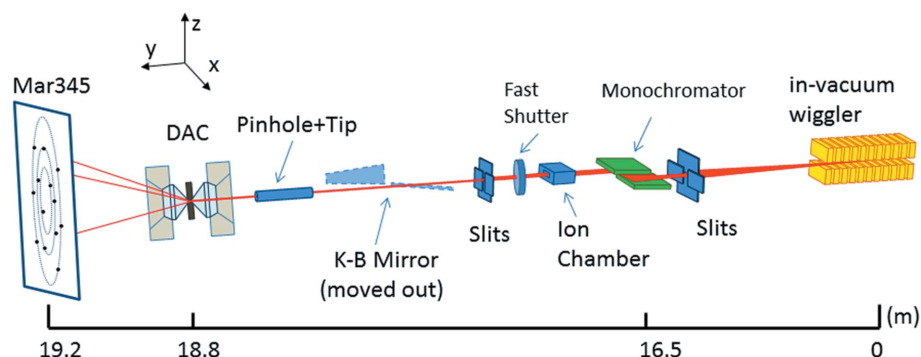

Figure 1
Schematic of beamline 4W2 at BSRF.

Table 2
Specifications of the in-vacuum wiggler of 4W2.

Source type	In-vacuum wiggler
Period length (m)	0.148
Period number	11
Peak magnetic field intensity (T)	1.5
Working gap range (mm)	14–120
Critical energy (keV)	7.48

receives radiation from an in-vacuum multi-period wiggler, the specifications of which are given in Table 2. The beam in the energy range 3.5–25 keV is then monochromated by a water-cooled Si(111) double-crystal monochromator at a distance of 16.5 m from the source. The energy of the electrons of BSRF is only 2.5 GeV, so the flux of the beam decreases drastically in the high energy range, as shown in Figure S1 of the supporting information. Using X-rays with higher energy will be helpful in increasing the accessible reciprocal volume and reducing the absorption by diamond anvils. As a compromise between beam energy and beam flux, X-rays of 20 keV (corresponding to a wavelength of 0.6199 Å) are usually selected as the incident beam for our single-crystal experiments. The energy of the incident beam is calibrated by scanning the *K*-edge of Mo.

A slit with dimensions 1.0 mm (H) × 1.2 mm (V) is mounted upstream of the monochromator to limit the size of the beam irradiating onto it. An ion chamber is mounted downstream of the monochromator to monitor the beam intensity. The intensity detected by the ion chamber is recorded during the exposure process, and subsequently used to correct the intensity of the collected reflections. The ion chamber is followed by an XRS6 fast shutter from Uniblitz® to control precisely the exposure time during data collection. Another slit is used downstream of the fast shutter to further limit the beam size to 50 µm × 50 µm. A tip of diameter 2 mm and length 50 mm was mounted near the DAC. After passing through a pinhole with a diameter of 50 µm at the exit of the tip, the X-ray beam intersects the axis of the ω-rotation stage at a certain point, which is termed the rotation centre with reference to a regular laboratory instrument. The tip and pinhole not only effectively remove the stray light in the ambient environment but also limit the beam to the desired size. The total distance from the source to the sample is 18.75 m. Due to such a rather short distance, in high-pressure powder diffraction experiments, a Kirkpatrick–Baez (KB) focusing mirror is positioned in the immediate vicinity of the sample to achieve a small beam size with high flux. Unfortunately, this configuration will result in a large convergence angle of the focusing beam. In the apparatus for high-pressure single-crystal diffraction, only the slit and pinhole are adopted to form a small beam size. KB focusing mirrors are abandoned to avoid broadening of diffraction spots, that result from the beam convergence. Additionally, the scattering power of single-crystalline samples is orders of magnitude higher than that of powder samples; diffraction data with sufficiently high signal-to-noise ratios may be attained even without using KB mirrors to improve the flux of the incident beam.

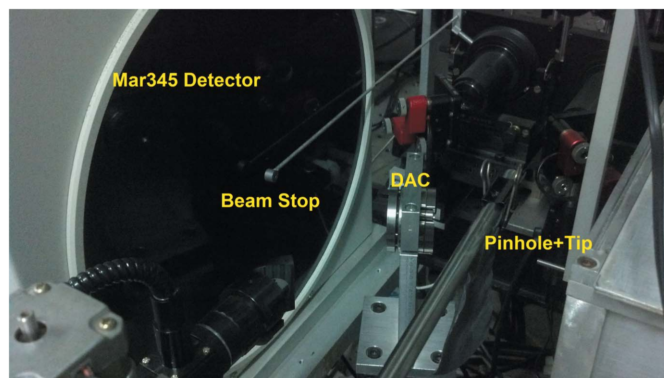

Figure 2
Experimental setup around the sample stage.

A photograph of the experimental setup around the sample stage is shown in Fig. 2.

To collect the diffraction data, the single-crystalline sample is first loaded into the DAC which is specially optimized for single-crystal diffraction. The DAC is then mounted on a stage which can move in three mutually perpendicular directions. Subsequently, the sample is positioned at the rotation centre with a precision better than 1 µm by adjusting the stage and rotation-scanning the crystal alternately. The position of the crystal is checked before data collection at each pressure. The rotation centre is also taken as the reference point to determine the sample–detector distance. The beam size at the sample position is 50 µm × 50 µm, much larger than a typical sample size (usually less than 20 µm × 20 µm × 10 µm) and positioning precision, so that consistent and reliable diffraction data can be recorded. After being correctly positioned at the rotation centre, the crystal rotates along a vertical axis to allow data collection at each desired orientation.

A Mar345 image plate is adopted as the detector. Although CCDs allow for faster readouts, image plates have a lower electronic noise and can achieve better signal-to-noise ratios. In addition, a large effective detective area is more attainable for image plates. For example, the Mar345 image plate has an effective detective area as large as 345 mm in diameter. The detective area of a typical CCD is in the range 75–165 mm in diameter. The large detective area allows for more reflections to be recorded per exposure. Limited by the small detective area, CCDs have to be placed at different positions to collect all the diffraction data which can be recorded by a fixed Mar345. This will significantly increase the complexity of the system. The pixel size of the Mar345 is 100 µm × 100 µm. In a typical experiment, the intensity of each reflection is distributed across several pixels. This benefits retrieval of diffraction intensities in the subsequent data processing. The distance from the sample to the image plate is about 185 mm, corresponding to a resolution limit of 0.83 Å. We also have a Pilatus3 2M detector available at beamline 4W2. Although the Pilatus3 2M is much faster than the Mar345, it has much larger pixels (172 µm × 172 µm), which will deteriorate the spatial resolution of the reflection spots. In addition, the Pilatus3 2M has a higher proportion of inactive area (8%) than the

Mar345. Due to the shadowing effect of the DAC, the accessible reciprocal volume is very limited in high-pressure single-crystal diffraction measurements. The high proportion of inactive area will further deteriorate the completeness and redundancy of diffraction datasets. Therefore, we use a Mar345 rather than a Pilatus to collect the single-crystal diffraction data.

3. Technical details

3.1. Workflow of high-pressure single-crystal diffraction measurement and overview of experimental setup

Collecting a diffraction dataset from a single crystal under high pressure is not so different from data collection using a regular laboratory instrument. First, the crystal is loaded and properly aligned. Then, a preliminary check is performed to evaluate the crystal quality and find the proper parameters for data collection. Subsequently, the diffraction data are collected. After indexing, integrating of reflections and applying a series of corrections, a dataset suitable for structure determination and refinement is finally obtained. A software package, *HPSXRD*, has been developed for the high-pressure single-crystal diffraction system, which not only controls the data acquisition but also implements indexing, integrating and correction of reflections. Finally, the diffraction dataset is exported as a data file in *SHELX* ∗.hkl format, which may be input into other programs for structure determination and refinement. A flow chart of the high-pressure single-crystal diffraction measurement and the main functions of the *HPSXRD* package are shown in Fig. 3.

The *HPSXRD* package is based on a Windows platform, and accessible for external users. Usually the external users can learn to use *HPSXRD* in a few minutes with the help of an easy-to-understand graphical user interface (GUI).

Some specific technical details of our system are given below.

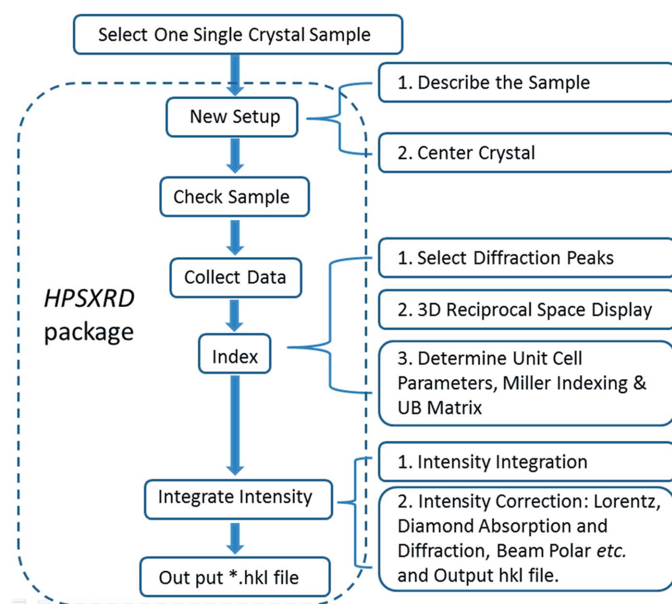

Figure 3
Flow chart of the high-pressure single-crystal diffraction experiment and main functions of the *HPSXRD* package.

3.2. DAC for single-crystal diffraction

The most significant characteristic of high-pressure single-crystal diffraction, which distinguishes it from regular single-crystal diffraction, lies in the crystal to be investigated having to be loaded into a DAC. Modifications have been made on commonly used symmetric DACs to obtain a wider accessible angular range. Anvils and seats of Boehler design (Boehler & Hantsetters, 2004) were adopted to achieve a large opening angle. The large opening angle is favourable for alleviating the shadowing effect of DACs, and collecting as many reflections as possible. On the other hand, it reduces the maximum attainable pressure applied to the sample. An opening angle of 70° was adopted as a compromise between the attainable diffraction range and maximum pressure. With such an opening angle, the DAC will not block the incident or diffracted X-ray beam even when the crystal rotates up to ±30° along the vertical axis. Because the beam size is 50 µm × 50 µm, the dimensions of the sample should be strictly limited to be compatible with the beam size. Samples with dimensions of less than 20 µm are preferred, and can be fully covered by the beam in the process of data collection. Then the scattering volume remains constant during the data collection. The constant scattering volume is convenient for the subsequent data processing. Diamond anvils with a culet diameter of 250–300 µm are usually adopted. Inert gas, such as Ar, Ne or He, is filled into the sample hole of the gasket as a pressure medium to provide a quasi-hydrostatic environment. Meanwhile, a ruby is loaded together with the sample as a pressure marker.

3.3. Indexing of reflections

In a few cases, samples from external users are aggregations of several crystallites rather than a real single-crystal. More frequently, single crystals are crushed into small pieces under high pressure. In both cases, the collected reflections come from several crystals at random orientation with respect to each other rather than a real single-crystal. This imposes great difficulties on the indexing of reflections. The well developed methods for the indexing of regular single-crystal data, such as the Niggli reduction method (Křivý & Gruber, 1976; Andrews & Bernstein, 1988) and the Fourier transform method (Steller *et al.*, 1997; Rossmann, 2006), cannot be applied directly to index such data. Therefore, a new protocol to index such diffraction data has been proposed (Li *et al.*, 2013).

3.4. Integration of diffraction data

A few methods have been developed to determine the intensity numerically of each diffraction spot collected using a two-dimensional detector. In general, these methods can be classified into two distinct types. One method is to fit the shape of a diffraction peak using a two-dimensional function and then determine the intensity of a reflection by integrating the

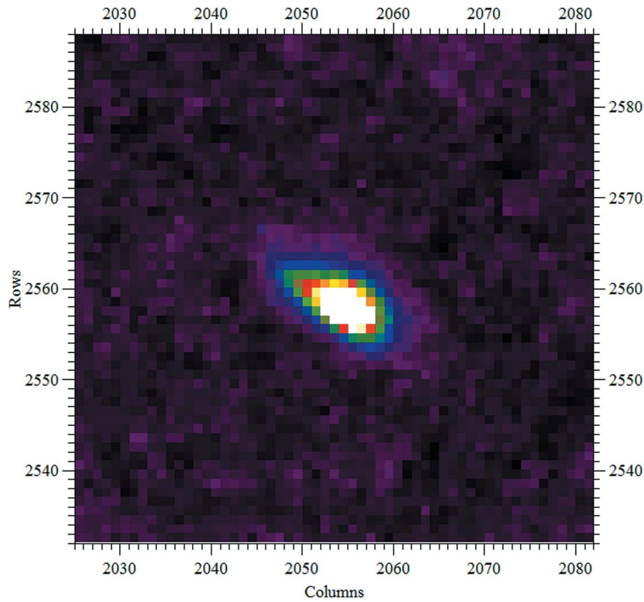

Figure 4
A typical diffraction spot collected by image plate in high-pressure single-crystal diffraction measurements. Sample: Cr_2O_3; pressure: 50.7 GPa; pressure medium: Ne.

corresponding function (Dera *et al.*, 2013). Nevertheless, this method is only applicable to diffraction peaks with a regular shape. The diffraction spots recorded in high-pressure single-crystal diffraction measurements are usually very distorted due to the presence of stress (Fig. 4), so can hardly be well fitted using a function. The other method is to analyse each diffraction spot statistically and determine its background level. Then the intensity of a certain reflection is obtained by subtracting the background from the total counts (Leslie, 2006). This method is applicable to the distorted diffraction spots, so is chosen in *HPSXRD* to determine the intensity of reflections.

The detailed procedure of determining the intensity of a diffraction spot implemented in *HPSXRD* is as follows. First, a region including N pixels around a Bragg position is delimitated. Then the average counts over the whole region, A_1, are calculated,

$$A_1 = \frac{\sum_i^N P_i}{N}, \quad (1)$$

where P_i is the counts at the ith pixel and N is the number of pixels in the whole region.

Afterwards, the average counts over all the pixels with counts less than A_1 are calculated as A_2,

$$A_2 = \frac{\sum_j^M P_j}{M} \left(P_j \leq A_1\right), \quad (2)$$

where P_j is the counts at the jth pixel and M is the number of pixels with counts less than A_1.

The intensity of a reflection is defined as

$$I_{\rm net} = \left[\sum_i^{N-M} P_i\right] - (N-M)\,A_2 \qquad (P_i > A_2). \quad (3)$$

The above algorithm is similar to that implemented in early instruments, such as the Enraf–Nonius CAD-4 diffractometer, for integrating the intensity of reflections detected by point detectors.

An example is given in §2 of the supporting information to illustrate how the intensity of a reflection is calculated in the *HPSXRD* package.

3.5. Lorentz-polarization factor and correction for DAC attenuation

During the data collection, the crystal rotates along the vertical axis at a constant angular velocity ω, resulting in different linear velocities at which the corresponding reciprocal lattice points go through the sphere of reflection (Ewald's sphere). The difference in exposure time among various reflections is taken into account by the Lorentz factor. Holton & Frankel (2010) have derived the Lorentz factor for the case in which the crystal rotation axis is perpendicular to the X-ray beam, given by

$$\mathrm{L} = \frac{1}{\left(\sin^2 2\theta - \zeta^2\right)^{1/2}}, \quad (4)$$

$$\zeta_\perp = \cos 2\theta \, Z_{\rm det}/X_{\rm stf},$$

where θ is the Bragg angle, ζ is a normalized projection of the reciprocal lattice point vector onto the rotation axis (z), $\zeta_\perp$ is ζ in terms of spot coordinates on a flat detector normal to the incident beam, $Z_{\rm det}$ is the coordinate of the diffraction spot on the detector along the axis parallel to the rotation axis (relative to the beam center in mm) and $X_{\rm stf}$ is the sample-to-detector distance along the direct-beam path (in mm). In our case, the Lorentz factor is reduced to a more simple form,

$$\mathrm{L} = D_M/Y, \quad (5)$$

where D_M is the distance from the rotation centre to the diffraction spot on the detector, and Y is the horizontal coordinate of the diffraction spot on the detector.

The X-ray beam striking the sample is polarized due to the nature of synchrotron radiation and the reflection by monochromator crystals. The polarization factor applicable to such a case has been derived by Kahn *et al.* (1982), and is adopted in *HPSXRD* directly. The polarization factor P derived by Kahn *et al.* is

$$P = P_0 - P' = \frac{1}{2}\left(1 + \cos^2 2\theta\right) - \frac{1}{2}\left(\mathcal{I}\cos 2\rho \sin^2 2\theta\right), \quad (6)$$

where θ is the Bragg angle of a reflection and ρ is the angle between the horizontal axis (y axis) of the detector and the line going through the reflection and the transmitted spot. Both θ and ρ are illustrated in Fig. 5. $\mathcal{I}$ is a parameter dependent on both the polarization of the synchrotron radiation source and the Bragg angle of the monochromator crystal, which may be deduced by fitting the background measured on the detector.

Before striking the sample, the X-ray beam has to go through the upstream diamond anvil, which is actually a

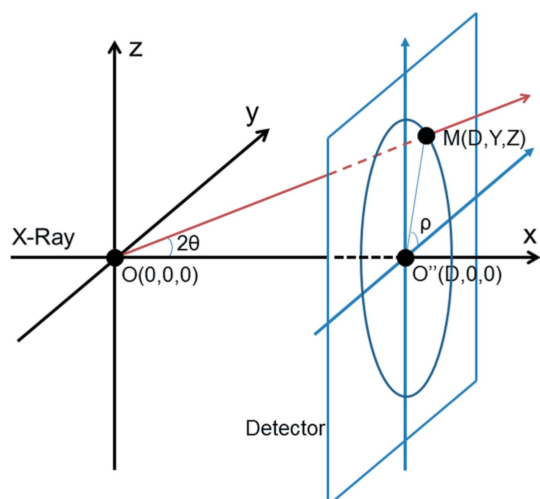

Figure 5
Diffraction geometry and parameters of the polarization correction.

millimetre-scale single-crystal. The X-ray beam will be attenuated owing to absorption and diffraction by the upstream diamond anvil, and the detected diffraction intensities have to be corrected to take into account this attenuation. Before or after the data collection, the intensity of the transmitted beam going through the upstream diamond anvil should be recorded at various ω angles. A typical plot of the intensities of the transmitted beam *versus* ω is shown in Fig. 6. At some particular ω angles, the transmitted beam is strongly attenuated due to the diffraction by the upstream diamond anvil. The envelope of the curve reveals the effect of absorption by the upstream anvil on the intensity of the transmitted beam. Such a curve as that shown in Fig. 6 can be used to correct the directly detected intensities because at each ω angle the orientation of the upstream diamond anvil for data collection is the same as that for recording the curve.

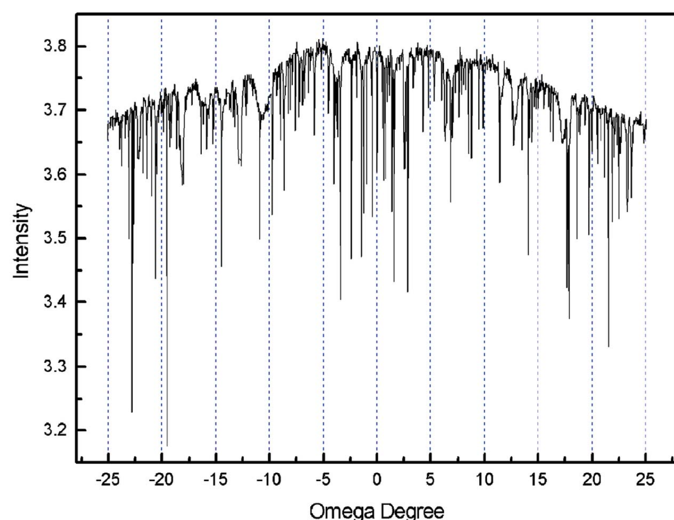

Figure 6
Intensity of the transmitted beam going through the upstream diamond anvil at various ω angles.

Owing to the absorption and reflection, the diffracted beam is further attenuated by the downstream diamond anvil. The attenuation is taken into account by calculating the path of a certain diffracted beam in the downstream diamond anvil. The attenuation due to the diffraction by the downstream diamond anvil is very complicated, and a method to compensate for it has not been developed yet. Fortunately, this attenuation seems to be insignificant, as revealed by the sample dataset presented in the following section.

4. Sample dataset

The experimental system, including the hardware and software, was validated using a crystal of LaB_6 as a reference. Datasets were collected in a pressure range from ambient pressure up to 39.1 GPa. The experiment was performed in a single-crystal DAC with 250 µm-diameter culets. A single crystal of size 20 µm × 20 µm × 25 µm was loaded into a 70 µm-diameter sample hole in a pre-indented stainless steel gasket with a thickness of 30 µm. Ne was filled into the sample chamber using a home-made compressed-gas loading system as a pressure medium to provide a quasi-hydrostatic environment. Ruby chips were used for pressure calibration (Mao *et al.*, 1986). Reflections were collected by ω scan in the range from −25° to 25°. Diffraction patterns were recorded at 2° intervals of ω. Each frame was exposed for 30 s. The result of a continuous ω scan is shown in Fig. 7 to give readers a direct impression of the diffraction data collected under high pressures. The resultant datasets were applied appropriate corrections and then input into *SHELXL97* (Sheldrick, 2008)

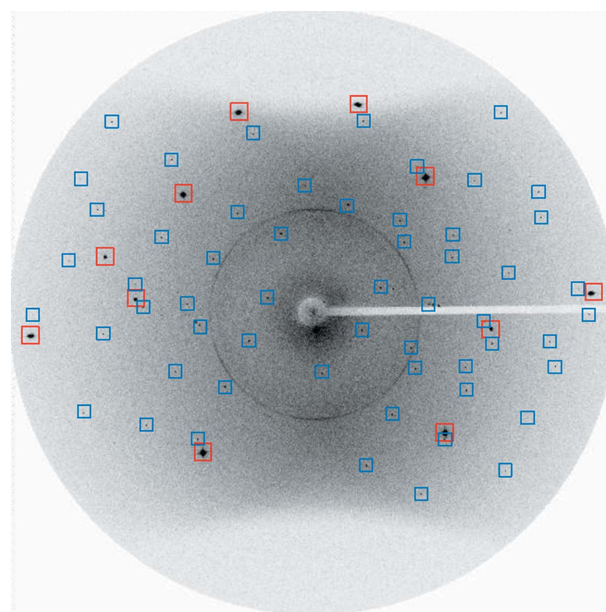

Figure 7
Diffraction data of LaB_6 collected under a pressue of 4.6 GPa. Reflections marked with red squares come from the diamond anvil and those marked with blue squares are reflections from LaB_6. The data were collected in a continuous ω scan in the range from −25 to 25° with an exposure time of 300 s.

Table 3
Lattice parameters and structure refinement parameters of LaB_6 at various pressures.

Pressure (GPa)	0.1 MPa	4.6	6.9	13.1	17.4
Lattice parameters (Å)	4.1581 (3)	4.1235 (4)	4.1086 (5)	4.0683 (4)	4.0446 (5)
Reflections collected/unique	120/23	55/20	51/20	51/19	51/20
R_{int}	0.0441	0.0452	0.0507	0.0255	0.0280
Completeness (%)	100	90.9	90.7	86.4	90.9
Data/restraints/parameters	23/0/5	20/0/5	20/0/5	19/0/5	20/0/5
Goodness-of-fit on F^2	1.270	1.382	1.281	1.208	1.228
Final R indices $R1$	0.0112	0.0154	0.0253	0.0119	0.0131
$wR2$	0.0291	0.0350	0.0620	0.0254	0.0289
Largest diffraction peak and hole (e Å^{-3})	0.37/−0.34	0.40/−0.91	0.58/−1.02	0.26/−0.52	0.30/−0.68
Pressure (GPa)	22.3	26.7	29.5	34.2	39.1
Lattice parameters (Å)	4.0176 (4)	3.9958 (4)	3.9798 (6)	3.9583 (5)	3.9387 (5)
Reflections collected/unique	48/18	45/18	46/18	43/17	46/18
R_{int}	0.0375	0.0435	0.0390	0.0401	0.0568
Completeness (%)	81.8	81.8	81.8	85.0	85.7
Data/restraints/parameters	18/0/5	18/0/5	18/0/5	17/0/5	18/0/5
Goodness-of-fit on F^2	1.271	1.350	1.408	1.363	1.407
Final R indices $R1$	0.0125	0.0222	0.0182	0.0187	0.0191
$wR2$	0.0236	0.0547	0.0489	0.0402	0.0405
Largest diff. peak and hole (e Å^{-3})	0.24/−0.38	0.48/−1.20	0.77/−0.52	0.50/−0.86	1.00/−0.52

to refine the structure. The results of the refinement are summarized in Table 3. B_0 = 179 ± 2 GPa and B_0' = 3.6 ± 0.1 are derived by fitting the experimental data with a third-order Birch–Murnaghan equation of state. The parameters of B_0 and B_0' obtained in this work agree better with the theoretically predicted values (Gürel & Eryiğit, 2010) than those derived in previous studies (Teredesai *et al.*, 2004; Godwal *et al.*, 2009), as shown in Table 4 and Fig. 8. As shown in Fig. 8, the observation points obtained in this study coincide with the fitted line very well, and the fitted line also agrees well with the theoretically predicted one. As indicated by the low R-factors of the refinement shown in Table 3, the datasets of LaB_6 are of high quality, which makes it feasible to retrieve the electron density from these datasets by the maximum entropy method. Further details about the dependence of the electron density distribution of LaB_6 on pressure will be reported elsewhere.

Table 4
Parameters of B_0 and B_0' derived in this and previous studies.

ME: methanol–ethanol mixtures in 4:1 ratio. MEW: methanol–ethanol–water mixtures in 16:3:1 ratio.

	Teredesai *et al.* (2004)	Godwal *et al.* (2009)		Gürel & Eryiğit (2010)	This work
Pressure medium	ME	Ar	MEW		Ne
V_0 (Å^3)	71.68	–	–	71.34	71.89
B_0	142 ± 15	173 ± 7	164 ± 2	180	179 ± 2
B_0'	4	4.2 ± 1.5	4.0 ± 0.4	3.79	3.6 ± 0.1

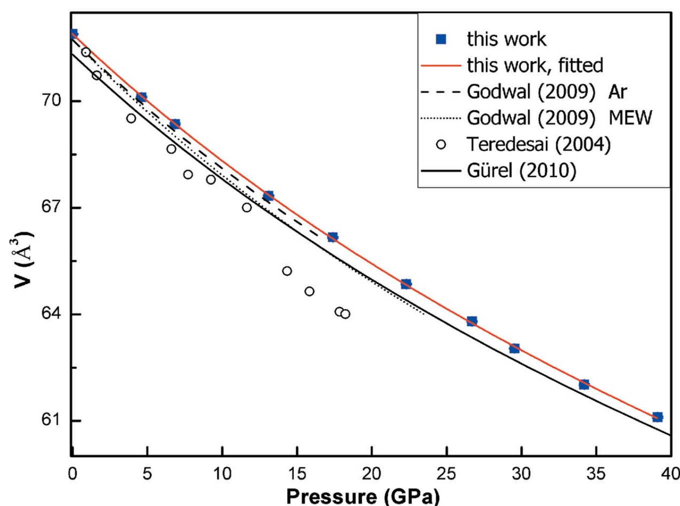

Figure 8
Dependence of unit-cell volume of LaB_6 on pressure. The black solid curve is a theoreticaly predicted result while other lines are obtained by fitting the experimental observations with the Birch–Murnaghan equation of state.

5. Conclusion

An experimental system has been set up at beamline 4W2 of BSRF to implement high-pressure single-crystal diffraction. In comparison with the regular laboratory instruments for single-crystal diffraction, the facility reported here has additional difficulties in designing, developing and data processing. Solutions for the major technical challenges are presented. The facility was validated using a crystal of LaB_6. The quality of the resultant dataset is found to be sufficient for structure solution and refinement. In addition, we also hope to develop a facility for low-temperature high-pressure single-crystal diffraction techniques in the near future.

Acknowledgements

We are grateful to Director Guoyin Shen (High Pressure Collaborative Access Team, Carnegie Institution of Washington) for advice on the system setup. The authors are grateful to Professor Meng He (National Centre of Nanoscience and Technology, China) for his help in preparing the manuscript.

Funding information

Funding for this research was provided by: National Natural Science Foundation of China (award Nos. 11274030, 11474281).

References

Akahama, Y. & Kawamura, H. (2010). *J. Phys. Conf. Ser.* **215**, 012195.
Andrews, L. C. & Bernstein, H. J. (1988). *Acta Cryst.* A**44**, 1009–1018.

Angel, R. J. (2004). *J. Appl. Cryst.* **37**, 486–492.
Angel, R. J. & Finger, L. W. (2011). *J. Appl. Cryst.* **44**, 247–251.
Angel, R. & Gonzalez-Platas, J. (2013). *J. Appl. Cryst.* **46**, 252–254.
Boehler, R. & De Hantsetters, K. (2004). *High. Press. Res.* **24**, 391–396.
Chen, B., Penwell, D., Nguyen, J. H. & Kruger, M. B. (2004). *Solid State Commun.* **129**, 573–575.
Dera, P., Lavina, B., Meng, Y. & Prakapenka, V. B. (2011). *J. Solid State Chem.* **184**, 3040–3049.
Dera, P., Zhuravlev, K., Prakapenka, V., Rivers, M. L., Finkelstein, G. J., Grubor-Urosevic, O., Tschauner, O., Clark, S. M. & Downs, R. T. (2013). *High. Press. Res.* **33**, 466–484.
Godwal, B. K., Petruska, E. A., Speziale, S., Yan, J., Clark, S. M., Kruger, M. B. & Jeanloz, R. (2009). *Phys. Rev. B*, **80**, 172104.
Gürel, T. & Eryiğit, R. (2010). *Phys. Rev. B*, **82**, 104302.
Hazen, R. M., Mao, H. K., Finger, L. W. & Hemley, R. J. (1987). *Phys. Rev. B*, **36**, 3944–3947.
Hemley, R. J., Bell, P. M. & Mao, H. K. (1987). *Science*, **237**, 605–612.
Holton, J. M. & Frankel, K. A. (2010). *Acta Cryst.* D**66**, 393–408.
Kahn, R., Fourme, R., Gadet, A., Janin, J., Dumas, C. & André, D. (1982). *J. Appl. Cryst.* **15**, 330–337.
Katrusiak, A. (2008). *Acta Cryst.* A**64**, 135–148.
Křivý, I. & Gruber, B. (1976). *Acta Cryst.* A**32**, 297–298.
Lager, G. A., Downs, R. T., Origlieri, M. & Garouttte, R. (2002). *Am. Mineral.* **87**, 642–647.
Leslie, A. G. W. (2006). *International Tables for Crystallography*, Vol. F, 1st online ed., ch. 11.2, pp. 212–217. Chester: International Union of Crystallography.
Li, H., Li, X., He, M., Li, Y., Liu, J., Shen, G. & Zhang, Z. (2013). *J. Appl. Cryst.* **46**, 387–390.
Li, R., Liu, J., Bai, L. G., Tse, J. S. & Shen, G. Y. (2015). *Appl. Phys. Lett.* **107**, 072109.
Li, Y. Ch., Lin, Ch. L., Li, G., Xu, J., Li, X. D. & Liu, J. (2014). *J. Appl. Phys.* **115**, 223507.
Lin, Ch. L., Zhang, Y. F., Liu, J., Li, X. D., Li, Y. Ch., Tang, L. Y. & Xiong, L. (2012). *J. Phys. Condens. Matter*, **24**, 115402.
Mao, H. K., Hemley, R. J., Chen, L. C., Shu, J. F., Finger, L. W. & Wu, Y. (1989). *Science*, **246**, 649–651.
Mao, H. K., Xu, J. & Bell, P. M. (1986). *J. Geophys. Res.* **91**, 4673–4676.
Mao, W. L., Mao, H. K., Sturhahn, W., Zhao, J., Prakapenka, V. B., Meng, Y., Shu, J., Fei, Y. & Hemley, R. J. (2006). *Science*, **312**, 564–565.
Mezouar, M., Crichton, W. A., Bauchau, S., Thurel, F., Witsch, H., Torrecillas, F., Blattmann, G., Marion, P., Dabin, Y., Chavanne, J., Hignette, O., Morawe, C. & Borel, C. (2005). *J. Synchrotron Rad.* **12**, 659–664.
Posner, E. S., Dera, P., Downs, R. T., Lazarz, J. D. & Irmen, P. (2014). *Phys. Chem. Miner.* **41**, 695–707.
Ridley, C. J. & Kamenev, K. V. (2014). *Z. Kristallogr.* **229**, 171–199.
Ross, N. L., Zhao, J. & Angel, R. J. (2004). *J. Solid State Chem.* **177**, 1276–1284.
Rossmann, M. G. (2006). *International Tables for Crystallography*, Vol. F, 1st online ed., ch. 11.1, pp. 209–211. Chester: International Union of Crystallography.
Rothkirch, A., Gatta, G. D., Meyer, M., Merkel, S., Merlini, M. & Liermann, H.-P. (2013). *J. Synchrotron Rad.* **20**, 711–720.
Shahar, A., Schauble, E. A., Caracas, R., Gleason, A. E., Reagan, M. M., Xiao, Y., Shu, J. & Mao, W. (2016). *Science*, **352**, 580–582.
Sheldrick, G. M. (2008). *Acta Cryst.* A**64**, 112–122.
Shen, G. & Sinogeikin, S. (2015). *Rev. Sci. Instrum.* **86**, 071901.
Sowa, H. & Ahsbahs, H. (2006). *J. Appl. Cryst.* **39**, 169–175.
Steller, I., Bolotovsky, R. & Rossmann, M. G. (1997). *J. Appl. Cryst.* **30**, 1036–1040.
Teredesai, P., Muthu, D. V. S., Chandrabhas, N., Meenakshi, S., Vijayakumar, V., Modak, P., Rao, R. S., Godwal, B. K., Sikka, S. K. & Sood, A. K. (2004). *Solid State Commun.* **129**, 791–796.
Watanuki, T., Machida, A., Ikeda, T., Ohmura, A., Kaneko, H., Aoki, K., Sato, T. J. & Tsai, A. P. (2007). *Philos. Mag.* **87**, 2905–2911.
Wu, L. Ch., Overgaard, J., Madsen, S. R., Schmøkel, M. S. & Brummerstedt Iversen, B. (2013). *J. Chin. Chem. Soc.* **60**, 929–934.
Xiao, W. S., Tan, D., Zhou, W., Chen, M., Xiong, X. L., Song, M. Sh., Liu, J., Mao, H. K. & Xu, J. (2012). *Am. Mineral.* **97**, 1193–1198.
Zhao, J., Angel, R. J. & Ross, N. L. (2010). *J. Appl. Cryst.* **43**, 743–751.